ISSN (Print) 1226-1750
ISSN (Online) 2233-6656
Journal of Magnetics 26(3), 299-304 (2021) https://doi.org/10.4283/JMAG.2021.26.3.299

Comparison of Image Quality According to Phantom Fluid Material in MR-based Attenuation Correction PET Imaging in PET/MR

Chan Rok Park*

Department of Radiological Science, Jeonju University, 303, Cheonjam-ro, Wansan-gu, Jeonju 55069, Republic of Korea

(Received 7 July 2021, Received in final form 29 September 2021, Accepted 29 September 2021)

Integrated positron emission tomography (PET)/magnetic resonance (MR) imaging is gradually being used to improve the rate of cancer lesion detection in the medical field. To enhance the quality of PET/MR images, attenuation correction (AC) techniques are used by applying MR pulse sequences of the controlled aliasing in parallel imaging results in higher acceleration (CAIPI; MR $AC_{Dixon\text{-}Caipi}$) and the generation autocalibrating partially parallel acquisition (GRAPPA; MR $AC_{Dixon\text{-}Grappa}$), based on the T1-weighted two-point Dixon pulse sequence. In addition, quality control using a Jaszczak phantom filled with water and radioisotopes is frequently performed when scanning the patient. When acquiring MR-based AC PET images in the phantom study, artifacts are caused by high permittivity in water, and there is a limitation in the acquisition of uniform image quality. Therefore, the purpose of this study was to compare the image quality using phantom fluids with lower permittivity than water (sodium chloride (NaCl) NaCl+nickel sulfate ($NiSO_4$)) according to MR $AC_{Dixon\text{-}Caipi}$ and MR $AC_{Dixon\text{-}Grappa}$ pulse sequences using various quantitative analysis parameters: percent of non-uniformity (PNU), percent contrast recovery (PCR), signal to noise ratio (SNR), and coefficient of variation (COV). The results indicated that the image quality with NaCl+$NiSO_4$ fluid based on the results was 1.2-, 1.6-, 1.4-, and 1.1 times superior to that of NaCl fluid, respectively. In conclusion, NaCl+$NiSO_4$ fluid is suitable as a phantom fluid material in PET/MR images.

Keywords : PET/MR, phantom fluid material, quality control, nuclear medicine image, attenuation correction, dixon pulse sequence, Controlled aliasing in parallel imaging results in higher acceleration (CAIPI) pulse sequence, Generation autocalibrating partially parallel acquisition (GRAPPA) pulse sequence

1. Introduction

Hybrid scanners, which combine multimodalities such as positron emission tomography (PET)/magnetic resonance (MR), play an important role in the field of nuclear medicine [1-3]. PET/MR has potential diagnostic advantages. Compared with PET/computed tomography (CT), patients can reduce radiation exposure and acquire excellent soft tissue information, particularly in the fields of oncology, neurology, and cardiology through PET/MR scans [4, 5]. Recently, integrated PET/MR, which involves placing the detector in the magnetic field using avalanche photodiodes (APDs) material instead of photomultiplier tubes (PMTs) has been developed [6]. In principle, gamma rays from emitted patients are detected in scintillation crystals such as lutetium oxyorthosilicate (LSO), which is widely used to convert gamma rays to visible light. Finally, nuclear medicine images are obtained by changing visible light to electrical signals [7, 8].

The attenuation correction (AC) process is essential for nuclear medicine imaging systems, because gamma rays are attenuated while arriving from the object to the detector [9]. In PET/computed tomography (CT), PET images were corrected for attenuated lesions via Hounsfield units through CT by converting CT energy (70-80 keV) to PET energy (~511 keV) [10]. In PET/MR, a T1-weighted two-point Dixon pulse sequence, which is applied for two echo times to acquire in phase, out of phase, fat, and water images by dividing into the background, lungs, fat, and soft tissue, and is generally used for attenuation correction [11]. Park *et al.* reported that the MR-based AC PET image quality for percent image uniformity is 15.2 % better than that of non-MR-based AC PET images [12]. There are two extension attenuation correction techniques based on the T1-weighted two-point Dixon pulse sequence. The first is the generation auto-

*Corresponding author: Tel: +82-63-220-2220
Fax: +82-63-220-2054, e-mail: tigeaglepcr@jj.ac.kr

calibrating partially parallel acquisition AC algorithm (GRAPPA; MR $AC_{Dixon\text{-}Grappa}$), which is helpful for higher sensitivity and better spatial resolution in MR images [13]. Second, controlled aliasing in parallel imaging involves the use of a higher acceleration AC algorithm (CAIPIRINHA; MR $AC_{Dixon\text{-}Caipi}$) [14]. Compared with the MR $AC_{Dixon\text{-}Grappa}$ pulse sequence, the MR $AC_{Dixon\text{-}Caipi}$ pulse sequence can be used for acquisition with a shorter scan time (~9 s). Thus, this pulse sequence is useful for patients who are not able to hold their breath, and has recently been applied for attenuation correction.

Quality control (QC) in nuclear medicine imaging is critical. Ziegler *et al.* offered considerable information on the performance of PET/MR instrumentation using a nuclear medicine phantom according to the National Electrical Manufacturers Association (NEMA) protocol [15]. The Jaszczak phantom, which mixes water and radioisotopes, is commonly used. However, water leads to strong artifacts during the acquisition of MR-based AC PET images in 3.0T because of the high relative permittivity ($\varepsilon = 78.3$) [16-19]. P. S. Tofts reported that cylindrical water phantoms may cause nonuniform artifacts in images above a 0.5T magnetic field [19]. To acquire a uniform MR-based AC PET image in PET/MR, an alternative phantom fluid material is required.

Therefore, the purpose of this study was to compare MR-based AC PET image quality using phantom fluid materials with lower permittivity (sodium chloride (NaCl): $\varepsilon = 77.5$, NaCl+nickel sulfate ($NiSO_4$): $\varepsilon = 72.8$) than water fluid according to the MR $AC_{Dixon\text{-}Caipi}$ and MR $AC_{Dixon\text{-}Grappa}$ pulse sequence for AC techniques. The percent of non-uniformity (PNU), percent contrast recovery (PCR), signal-to-noise ratio (SNR), and coefficient of variation (COV) were used for quantitative analysis.

2. Materials and Methods

2.1 Experimental setup

Simultaneous PET/MR (Biograph mMR; Siemens) was used to acquire the MR AC PET images. The MR pulse sequences generated by generating attenuation correction PET images were MR $AC_{Dixon\text{-}Caipi}$ and MR $AC_{Dixon\text{-}Grappa}$ pulse sequences. The PET detector is located between the body radiofrequency (RF) coil and the gradient coil in a single gantry. The PET detector consisted of an 8×8 LSO scintillation crystal, eight detector rings, 56 detector blocks, and a 3×3 avalanche photodiode array. In addition, the Jaszczak PET phantom was used in our experiment by changing NaCl and NaCl+$NiSO_4$ fluids instead of water. According to the NEMA protocol, the ^{18}F solution was filled in the Jaszczak PET phantom and the radioactivity ratio between the spheres and background was maintained at 10:1 [20]. The experiments were implemented at a 3.0T magnetic field at 23 °C and ten times under equivalent conditions for expression of statistical analysis.

2.2 Quantitative analysis

To evaluate the image quality, the PNU, PCR, SNR, and COV were used for quantitative parameters. The regions of interest (ROIs) were drawn by acquisition of MR-based AC PET images, according to the formulae in Fig. 1. The PNU was calculated as follows:

$$\text{PNU}\ (\%) = 100 \times \frac{S_{maximum} - S_{average}}{S_{average}} \tag{1}$$

where $S_{maximum}$ and $S_{average}$ are the maximum count and average count for the ROIs in Fig. 1(a), respectively. The PCR for four spheres (31.8, 25.4, 19.1, and 15.1 mm) in Fig. 1(b) was calculated as follows:

$$\text{PCR}\ (\%) = \frac{\frac{J_{H,c}}{J_{B,c}} - 1}{\frac{r_H}{r_B}} \times 100 \tag{2}$$

Where the $J_{H,C}$ expresses the average counts for the sphere, which has the inner diameter, H. $J_{B,C}$ indicates 12

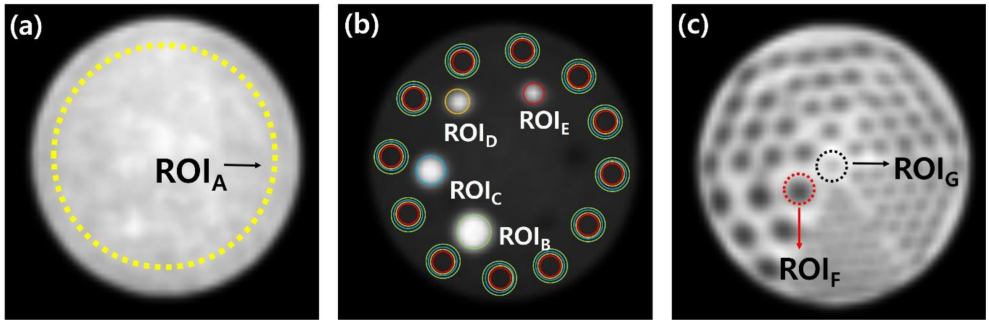

Fig. 1. (Color online) Images of various regions of interest (ROI) for percent of non-uniformity (PNU) using ROI_A, percent contrast recovery (PCR) using ROI_B, ROI_C, ROI_D, ROI_E corresponding to inner sphere sizes of 31.8, 25.4, 19.1, and 15.9 mm, respectively, signal-to-noise ratio (SNR) using ROI_F, and coefficient of variation (COV) using ROI_G.

average background counts in H mm of the sphere. r_H/r_B is the radioactivity ratio of the hot sphere to the background sphere. The ratio was maintained at 10:1 (sphere : background sphere = 10 : 1). In addition, the SNR and COV are given as:

$$\text{SNR} = \frac{S_C}{\sigma_C} \tag{3}$$

$$\text{COV} = \frac{\sigma_C}{S_C} \tag{4}$$

where S_C and σ_C are the average counts and standard deviation values, respectively. In this study, the SNR and COV results were applied to ROI_F and ROI_G, as shown in Fig. 1(c).

3. Results

Figs. 2 and 3 show the phantom images filled with NaCl and NaCl+$NiSO_4$ fluid after applying the MR $AC_{\text{Dixon-Caipi}}$ and MR $AC_{\text{Dixon-Grappa}}$ pulse sequences, respectively. Fig. 4 shows the PNU values according to the MR $AC_{\text{Dixon-Caipi}}$ and MR $AC_{\text{Dixon-Grappa}}$ pulse sequences. Based on the MR $AC_{\text{Dixon-Caipi}}$ pulse sequence results in Fig. 4(a), PNU is 17.1 and 13.3 % for NaCl and NaCl+$NiSO_4$ fluids, respectively. In addition, the PNU for the MR $AC_{\text{Dixon-Grappa}}$ pulse sequence in Fig. 4(b) is 17.2 and 14.9 % for NaCl and NaCl+$NiSO_4$ fluids, respectively. The PCR results based on the MR $AC_{\text{Dixon-Caipi}}$ and MR $AC_{\text{Dixon-Grappa}}$ pulse sequences according to the NaCl and NaCl+$NiSO_4$ fluids for 31.8, 25.4, 19.1, and 15.9 mm sphere sizes are shown in Fig. 5. Based on the results, the PCR valuses for 31.8, 25.4, 19.1, and 15.9 mm sphere sizes were 71.3, 65.1, 53.8, and 48.9 % for the MR $AC_{\text{Dixon-Caipi}}$ pulse sequence for NaCl fluid, 106.6, 102.4, 92.1, and 63.9 % for the MR $AC_{\text{Dixon-Caipi}}$ pulse sequence

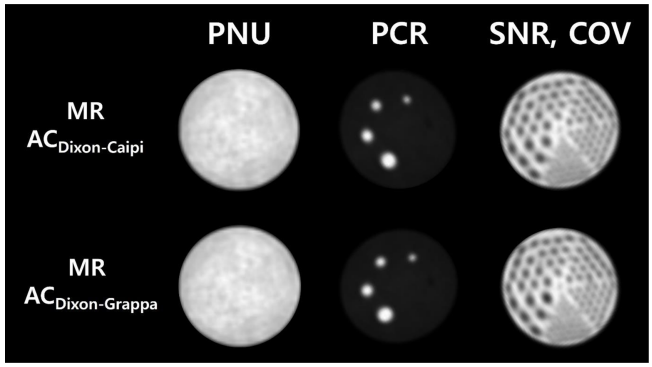

Fig. 2. Images using NaCl fluid material for MR $AC_{\text{Dixon-Caipi}}$ and MR $AC_{\text{Dixon-Grappa}}$ pulse sequences through quantitative analysis such as percent of non-uniformity (PNU), percent contrast recovery (PCR), signal-to-noise ratio (SNR), and coefficient of variation (COV).

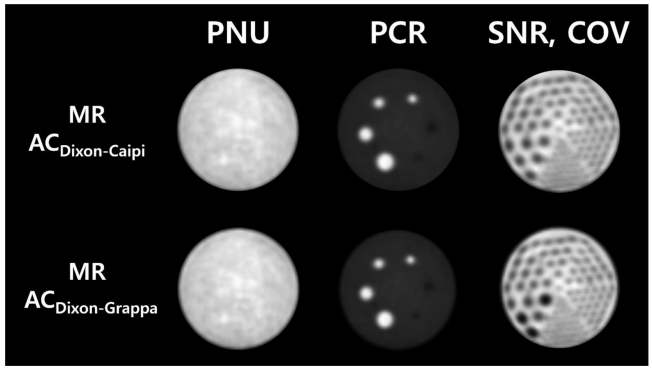

Fig. 3. Images using NaCl+$NiSO_4$ fluid material according to MR $AC_{\text{Dixon-Caipi}}$ and MR $AC_{\text{Dixon-Grappa}}$ pulse sequences through quantitative analysis such as percent of non-uniformity (PNU), percent contrast recovery (PCR), signal-to-noise ratio (SNR), and coefficient of variation (COV).

for NaCl+$NiSO_4$ in Fig. 5(a). In addition, the Fig. 5(b) showed that the PCR valuses for 31.8, 25.4, 19.1, and 15.9 mm sphere sizes were 71.6, 65.8, 52.3, and 48.6 %

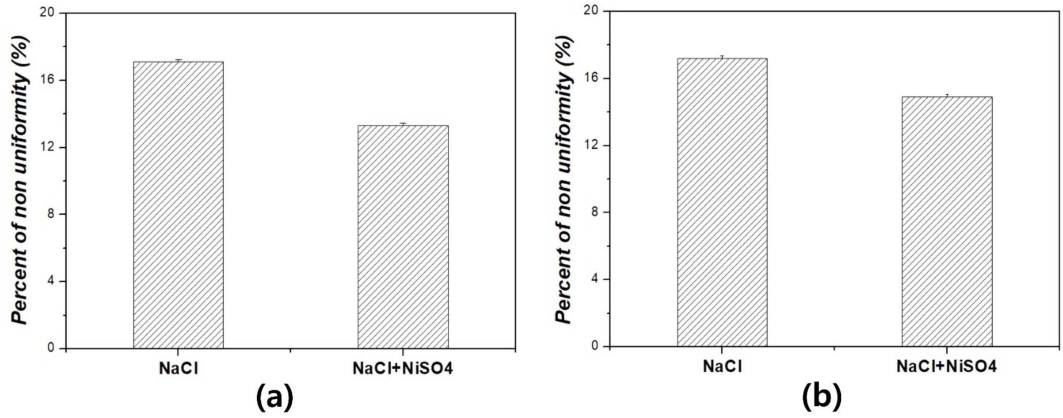

Fig. 4. Percent of non-uniformity (PNU) after replacing NaCl and NaCl+$NiSO_4$ fluid material according to (a) MR $AC_{\text{Dixon-Caipi}}$ and (b) MR $AC_{\text{Dixon-Grappa}}$ pulse sequences.

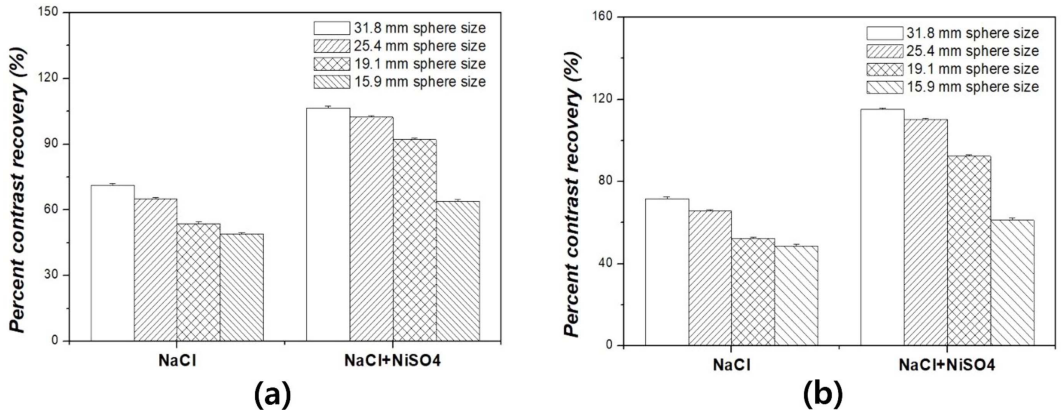

Fig. 5. Percent contrast recovery (PCR) at each inner sphere size after replacing the NaCl and NaCl+$NiSO_4$ fluid material according to (a) MR $AC_{Dixon\text{-}Caipi}$ and (b) MR $AC_{Dixon\text{-}Grappa}$ pulse sequences.

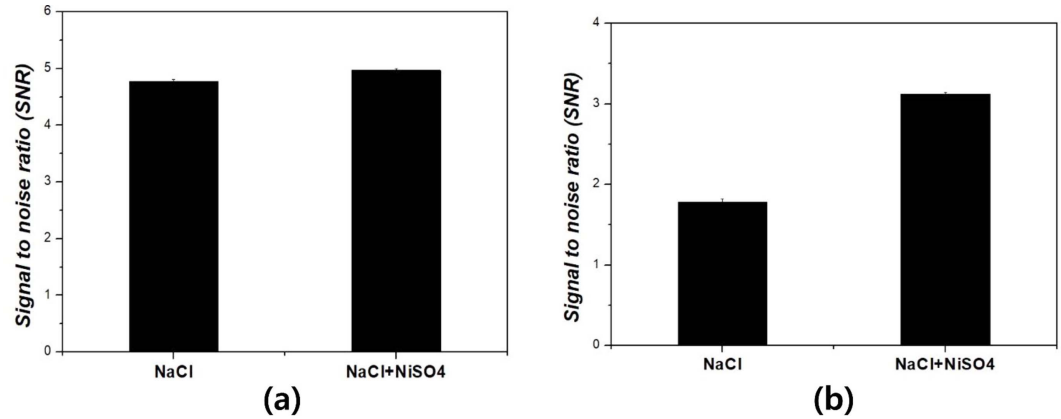

Fig. 6. Signal-to-noise ratio (SNR) after replacing the NaCl and NaCl+$NiSO_4$ fluid material according to (a) MR $AC_{Dixon\text{-}Caipi}$ and (b) MR $AC_{Dixon\text{-}Grappa}$ pulse sequences.

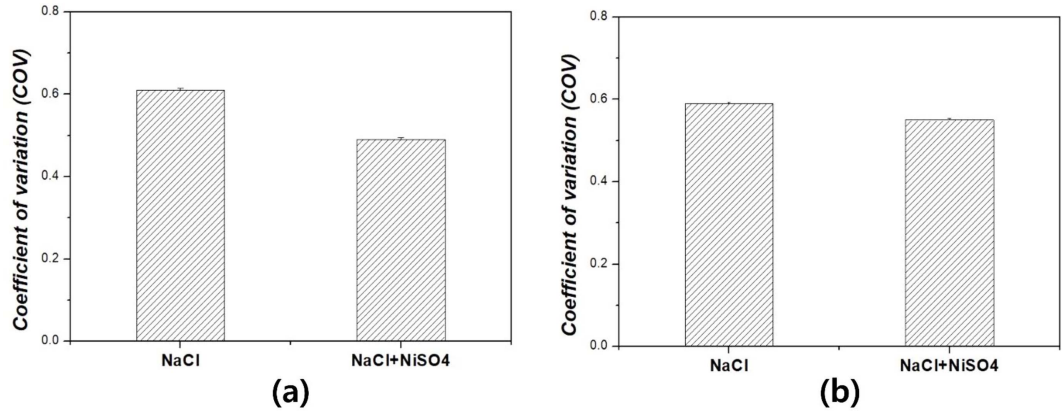

Fig. 7. Coefficient of variation (COV) after replacing the NaCl and NaCl+$NiSO_4$ fluid material according to (a) MR $AC_{Dixon\text{-}Caipi}$ and (b) MR $AC_{Dixon\text{-}Grappa}$ pulse sequences.

for the MR $AC_{Dixon\text{-}Grappa}$ pulse sequence with NaCl, 115.9, 110.2, 92.3, and 61.3 % for the MR $AC_{Dixon\text{-}Grappa}$ pulse sequence for NaCl+$NiSO_4$, respectively. For each sphere, the PCR results were, on average, 59.7 % and 93.1 % for NaCl and NaCl+$NiSO_4$ fluids, respectively, regardless of the MR AC pulse sequences. The SNR and COV values for the rod spheres are shown in Figs. 6 and 7, respectively. The SNR values according to NaCl

and NaCl+$NiSO_4$ fluids are 4.7 and 4.9 for the MR $AC_{Dixon\text{-}Caipi}$ pulse sequence in Fig. 6(a). The Fig. 6(b) showed that the SNR values according to NaCl and NaCl+$NiSO_4$ fluids 1.8 and 3.2 for the MR $AC_{Dixon\text{-}Grappa}$ pulse sequence. The COV values for MR $AC_{Dixon\text{-}Caipi}$ and MR $AC_{Dixon\text{-}Grappa}$ pulse sequences were 0.6 and 0.5 for NaCl and NaCl+$NiSO_4$ fluids in Fig. 7, respectively.

4. Discussion

Water, which is the most used phantom fluid, causes distortion in MR-based AC PET images in PET/MR because of the high permittivity in the 3.0T magnetic field. To overcome this limitation, we investigated the image quality when using NaCl and NaCl+$NiSO_4$ phantom fluids, which have low permittivity compared with that of water according to MR $AC_{Dixon\text{-}Caipi}$ and MR $AC_{Dixon\text{-}Grappa}$ pulse sequences.

Based on the PNU results in Fig. 4, the image quality with NaCl+$NiSO_4$ fluid was 1.3-and 1.2 times superior to that of the image with NaCl fluid for the MR $AC_{Dixon\text{-}Caipi}$ and MR $AC_{Dixon\text{-}Grappa}$ pulse sequences, respectively. Compared with NaCl and NaCl+$NiSO_4$ fluids for PNU according to MR $AC_{Dixon\text{-}Caipi}$ and MR $AC_{Dixon\text{-}Grappa}$ pulse sequence, PNU values based on the NaCl fluid were not different.

The image quality with NaCl+$NiSO_4$ fluid of PCR results for MR $AC_{Dixon\text{-}Caipi}$ pulse sequence in 31.8-, 25.4-, 19.1-, and 15.9 sphere sizes in Fig. 5(a) were 1.5-, 1.6-, 1.7-, and 1.3 times superior, respectively, than that with NaCl fluid. In addition, the image quality with NaCl+$NiSO_4$ fluid of PCR results for MR $AC_{Dixon\text{-}Grappa}$ pulse sequence in Fig. 5(b) was superior 1.6, 1.7, 1.8, and 1.3 fold that of the NaCl fluid. According to MR $AC_{Dixon\text{-}Caipi}$ and MR $AC_{Dixon\text{-}Grappa}$ pulse sequences, the image quality with NaCl+$NiSO_4$ fluids is 1.5-and 1.6 higher, respectively, than that of NaCl fluid. According to the PCR results for NaCl and NaCl+$NiSO_4$ fluids, there was no significant difference between MR $AC_{Dixon\text{-}Caipi}$ and MR $AC_{Dixon\text{-}Grappa}$ pulse sequences. The PCR values with NaCl+$NiSO_4$ fluid are 1.6 times higher than those with NaCl fluid on average.

Compared with the SNR results for the MR $AC_{Dixon\text{-}Caipi}$ pulse sequence between the NaCl and NaCl+$NiSO_4$ fluids in Fig. 6(a), the SNR values for the NaCl+$NiSO_4$ fluids were 1.1 higher than those of the NaCl fluid. The SNR value is also 1.8 higher than that of NaCl fluid for the MR $AC_{Dixon\text{-}Grappa}$ pulse sequence, as shown in Fig. 6(b). For the COV results in Fig. 7, COV values for the NaCl+$NiSO_4$ fluid were 1.2 and 1.1 times lower than those of NaCl fluid for MR $AC_{Dixon\text{-}Caipi}$ and MR $AC_{Dixon\text{-}Grappa}$ pulse sequences, respectively.

Research using a nuclear medicine phantom filled with water, such as the Hoffman 3D brain phantom, Jaszczak phantom, and quadrant bar phantom, was performed to evaluate and improve image quality. This study aimed to identify an alternative fluid material to water as a phantom in PET/MR. Ziegler *et al.* reported that there are various insensitive fluid materials in MR pulse sequences such as emulsions (75 % oil and 25 % water) and oil [19]. However, these materials are limited by the use of phantom fluids. Although these fluids can reduce image distortion due to low permittivity, these materials cannot mix radioisotopes and can cause air bubbles in the phantom. Therefore, a uniform phantom image cannot be acquired. In addition, several researchers have used NaCl +$NiSO_4$ fluid material when performing a phantom study to acquire PET/MR imaging [21, 22].

In this study, the MR-based PET images were acquired and evaluated by replacing the phantom fluid materials (NaCl and NaCl+$NiSO_4$ fluids), which have characteristic lower permittivity compared with water. Quantitative analysis was performed using PNU, PCR, SNR, and COV parameters. Before scanning the patient in the medical clinical field, the conformation of image quality through QC using a nuclear medicine phantom is essentially performed to improve the diagnostic rate for cancer lesions. Based on the quantitative analysis results, our results indicate that NaCl+$NiSO_4$ phantom fluid material is the best alternative to water.

We are going to consider that the following two future research. First of all, there is ultrashort echo time (UTE) pulse sequence, which is mostly used for brain AC in PET/MR [23, 24]. We need to compare the image quality in PET/MR images between Dixon and UTE AC pulse sequences. Second, additional phantom experiment can be performed using conventional fluid material such as water. Therefore, the comparison study is needed according to water, NaCl, NaCl+$NiSO_4$ phantom fluid materials, respectively.

5. Conclusion

Recently, integrated PET/MR scans have been broadly performed because they can simultaneously acquire functional and soft tissue information. They are also useful in reducing radiation exposure to patients. In addition, QC using a phantom, which is injected with water and radioisotopes, is implemented to maintain excellent image quality. However, water is inappropriate as a phantom fluid material because of its high permittivity in PET/MR images. Here, we compared PET image quality by chang-

ing phantom fluids (NaCl and NaCl+$NiSO_4$) according to MR AC pulse sequences (MR $AC_{Dixon\text{-}Caipi}$ and MR $AC_{Dixon\text{-}Grappa)}$, which are broadly applied to attenuation-corrected PET/MR images. In conclusion, the results of this study are valuable for the improvement of MR-based AC PET image quality using NaCl+$NiSO_4$ fluid than that with NaCl fluid.

References

[1] G. Delso, S. Fürst, B. Jakoby, R. Ladebeck, C. Ganter, S. G. Nekolla, M. Schwaiger, and S. I. Ziegler, J. Nucl. Med. **52**, 1914 (2011).

[2] S. Vandenberghe and P. K. Marsden, Phys. Med. Biol. **60**, R115 (2015).

[3] G. A. Bindseil, K. M. Gilbert, T. J. Scholl, W. B. Handler, and B. A. Chronik, Magn. Reson. Med. **66**, 301 (2011).

[4] N. Gross-Weege, T. Nolte, and V. Schulz, Phys. Med. Biol. **64**, 1 (2019).

[5] P. Jezzard, A. S. Barnett, and C. Pierpaoli, Magn. Reson. Med. **39**, 801 (1998).

[6] G. Delso and S. Ziegler, Eur. J. Nucl. Med. Mol. Imaing **36**, 86 (2009).

[7] G. Muehllehner and J. S. Karp, Phys. Med. Biol. **51**, R117 (2006).

[8] F. M. Bengel, S. I. Ziegler, N. Avril, W. Weber, C. Laubenbacher, and M. Schwaiger, Eur. J. Nucl. Med. **24**, 1091 (1997).

[9] P. E. Kinahan and D. W. Townsend, Med. Phys. **25**, 2046 (1998).

[10] T. Pan, O. Mawlawi, S. A. Nehmeh, Y. E. Erdi, D. Luo, H. H. Liu, R. Castillo, R. Mohan, Z. Liao, and H. A. Macapinlac, J. Nucl. Med. **46**, 1481 (2005).

[11] M. Eiber, T. Takei, M. Souvatzoglou, M. E. Mayerhoefer, S. Fürst, F. C. Gaertner, D. J. Loeffelbein, E. J. Rummeny, S. I. Ziegler, M. Schwaiger, and A. J. Beer, J. Nucl. Med. **55**, 191 (2014).

[12] C. R. Park and Y. Lee, Nucl. Eng. Technol. **51**, 1610 (2019).

[13] M. A. Griswold, P. M. Jakob, R. M. Heidemann, M. Nittka, V. Jellus, J. Wang, B. Kiefer, and A. Haase, Mag. Reson. Med. **47**, 1202 (2002).

[14] F. A. Breuer, M. Blaimer, M. F. Mueller, N. Seiberlich, R. M. Heidemann, M. A. Griswold, and P. M. Jakob, Mag. Reson. Med. **55**, 549 (2006).

[15] S. Ziegler, B. W. Jakoby, H. Braun, D. H. Paulus, and H. H. Quick, EJNMMI Phys. **2**, 1 (2015).

[16] P. S. Tofts, J. Magn. Reson. **104**, 143 (1994).

[17] H. P. Schwan, R. J. Sheppard, and E. H. Grat, J. Chem. Phys. **64**, 2257 (1976).

[18] A. Peyman, C. Gabriel, and E. H. Grant, Bioeletromagnetics **28**, 264 (2007).

[19] S. Ziegler, H. Braun, P. Ritt, C. Hocke, T. Kuwert, and H. Quick, J. Nucl. Med. **54**, 1464 (2013).

[20] National Electrical Manufacturers Association Performance measurements of positron emission tomography NEMA standard publication NU 2-2007 (2007).

[21] C. R. Park, K. Kim, and Y. Lee, Optik **178**, 161 (2019).

[22] B. Aklan, M. Oehmigen, K. Beiderwellen, M. Ruhlmann, D. H. Paulus, B. W. Jakoby, P. Ritt, and H. H. Quick, J. Nucl. Med. **57**, 78 (2016).

[23] L. B. Aasheim, A. Karlberg, P. E. Goa, A. Håberg, S. Sørhaug, U. Fagerli, and L. Eikenes, Eur. J. Nucl. Med. Mol. Imaging. **42**, 1439 (2015).

[24] V. Keereman, Y. Fierens, T. Broux, Y. D. Deene, M. Lonneux, and S. Bandenberghe, J. Nucl. Med. **51**, 812 (2010).